One step synthesis and sintering of Ni and Zn substituted tetrahedrite as thermoelectric material

S. Battiston[a]

C. Fanciulli[b]

S. Fiameni[a, *]

stefania.fiameni@cnr.it

A. Famengo[a]

S. Fasolin[a]

M. Fabrizio[a]

[a]CNR - ICMATE, Corso Stati Uniti 4, 35127, Padova, Italy

[b]CNR - ICMATE, Corso Promessi Sposi 29, 23900, Lecco, Italy

*Corresponding author.

Abstract

Tetrahedrite mineral family, one of the most widespread sulfosalts on Earth's crust, seems to meet the right features for an attractive sustainable p-type thermoelectric material, showing relatively high conversion efficiency. The sulphide powders were ball milled and then one-step simultaneous synthesis and sintering process was performed by open die pressing (ODP). This simple, fast, and easy scalable route was extensively discussed for the first time in this work and permitted to obtain thermoelectric pellets starting from sulphide precursors, with a whole process lasting less than 6 h. Both Zn and Ni cations were added as partial substituents of Cu in $Cu_{12}Sb_4S_{13}$ permitting to considerably improve the thermoelectric performances of the undoped material prepared by ODP. The influence of precursors ratio on the tetrahedrite phase, secondary phase content and stoichiometry were investigated by X-ray diffraction, scanning electron microscopy and energy dispersive X-ray spectroscopy. The density and mechanical stability of samples were evaluated as a function of the chemical composition and processing parameters. A complete thermoelectric characterization was carried out for samples with different Zn and Ni substitution up to 400 °C.

Keywords: Thermoelectrics; Tetrahedrite; Mineral; Geomimetic; Sintering

1 Introduction

The interest in thermoelectric materials raised in the recent years due to the possibility of designing thermoelectric generators (TEGs). TEG are reliable solid-state devices for waste heat recovery able to generate electricity where the employment of other technologies is not suitable. In this direction, the automotive market is making efforts in order to couple TEGs to combustion engines for improving the overall system efficiency exploiting the exhaust steam heat recovery [1].

Nowadays, one of the main challenge in the thermoelectric field seems to be the identification of efficient thermoelectric materials, which should be inexpensive, easy to synthesize, and comprised of earth-abundant elements. In this perspective, tetrahedrite mineral family, one of the most widespread sulfosalts on Earth's crust, seems to be an attractive sustainable source for p-type thermoelectric materials. Tetrahedrites show a relatively high figure of merit ZT ($ZT = \alpha^2\rho^{-1}\kappa^{-1}T$, where α is the Seebeck coefficient, ρ the electrical resistivity and κ the thermal conductivity) with values around unity at 450 °C [2,3]. This temperature is particularly suitable for waste heat recovery, the same supported by chalcogenides, representing an important material feature which people working on development of automotive thermoelectric applications are interested in. Minerals of the tetrahedrite series, ranging from $Cu(I)_{10}Cu(II)_2Sb_4S_{13}$ to $Cu(I)_{10}Cu(II)_2As_4S_{13}$ (tennantite), can easily host several kind of elements (such as Mn, Fe, Co, Ni, Zn, Pb, Cd, and Hg) and are often associated to gold, silver, and telluride ores. In particular, they are present in nature as single mineral (especially in America) and as accessory minerals in hydrothermal rocks (very common in

Europe), hardly separable by other sulphides (mainly pyrite and chalcopyrite) [4–6].

Nevertheless, working on the geomimetic synthetic tetrahedrites can deepen the knowledge about this material leading to understand how to enhance and exploit the natural mineral effectively. On the other hand, it is possible to tailor the material avoiding or limiting the presence of undesired toxic elements, such as Pb, Te and As, a crucial issue for those natural mineral thermoelectric materials.

By the crystallographic point of view, the cubic tetrahedrite phase, $Cu^{1+}_{10}\ Cu^{2+}_{2}\ Sb^{3+}_{4}\ S^{2-}_{13}$, possesses two different lattice sites Cu(1) and Cu(2) with sulphur atoms tetrahedrally and trigonally coordinated respectively. In general, the site Cu(1) is occupied for one third by the monovalent copper cations and two third by the bivalent ones, whilst the site Cu(2) is occupied only by the monovalent ones [7]. The low lattice thermal conductivity seems to be mainly related to the site Cu(2), whilst the substitution of the bivalent cations in the site Cu(1) mainly affects the electrical resistivity, thus decreasing the charge carrier contribution to the thermal conductivity [8–10].

The state of art for this material shows the best improvement in thermoelectric properties by the substitution of Cu^{2+} atoms with Ni and Zn. In particular, the ZT of tetrahedrite is reported to increase from about 0.6 (at 400 °C) up to 0.9 (at 447 °C) with Zn substitution [3], while a value of 0.7 (at 392 °C) was reached with Ni substitution [10]. Zn reduced the electrical conductivity of tetrahedrite, and consequently the electronic part of the thermal one. Introducing both the substituents, the best performance was achieved with a resulting ZT of almost 1 at 450 °C [11], making the tetrahedrite the polycrystalline thermoelectric material with the highest performance in this temperature range. In general, the synthetic routes reported in literature so far are multi-step processes mainly based on direct melting methods performed in vacuum, starting from pure elements and employing high temperatures (above 700 °C). The whole procedure can last from 54 h up to several weeks [3,10,12,13]. Recently, several authors addressed their efforts to develop simpler and shorter synthesis procedures for an easier industrial scale-up [6,14,15]. In particular, Barbier et al. were able to exploit their rapid synthesis route for a production of large tetrahedrite pellets ($Cu_{10.4}Ni_{1.6}Sb_4S_{13}$) employing spark plasma synthesis technique, with a resulting ZT of 0.75 at 427 °C [16].

On the basis of these considerations, in this work both Zn and Ni cations were employed as partial Cu^{2+} substituents, starting from the best reported thermoelectric performance stoichiometry ($Cu_{10.5}Ni_1Zn_{0.5}Sb_4S_{13}$) [11] and focusing on improving the procedure for a simple, scalable and fast route for mechanically stable thermoelectric tetrahedrite pellet. In particular, ball milling treatment of sulphide powder precursors and one-step reactive sintering method were performed by open die pressing (ODP) [17], with an overall duration of less than 6 h. The reactive sintering process was previously demonstrated to be effective for fast thermoelectric material production employing spark plasma sintering technique (SPS) [18,19]. With respect to the SPS, the ODP technique is cheaper (for instance, vacuum is not needed), permitting the sintering even of oxygen sensitive materials [20].

2 Material and methods

Ni-Zn substituted tetrahedrite materials were fabricated via solid state reaction of sulphide powder precursors and elemental sulphur to obtain four different $Cu_{10}Cu_{1-x}Ni_1Zn_xSb_4S_{13}$, stoichiometries with x = 0.0, 0.3, 0.5, 0.7. $Cu_{12}Sb_4S_{13}$ was also synthesized as reference (blank sample). Two series of samples for each stoichiometry were synthesized: in the second series, named Ni-rich samples, a 15 wt% excess of Ni_3S_2 was added as a Ni- binder additive.

CuS (Sigma Aldrich, 100 mesh, purity of 99%), Cu_2S (Sigma Aldrich, 100 mesh), Sb_2S_3 (Sigma Aldrich,), Ni_3S_2 (Sigma Aldrich, 150 mesh, purity of 99.7%), ZnS (Sigma Aldrich, 10 µm, purity of 99.99%), and S (Sigma Aldrich, 100 mesh, purified by sublimation) were mixed in the appropriate stoichiometry and processed in a planetary ball mill (Pulverisette 5, Fritsch) employing tungsten carbide balls and jar at 350 rpm, with a ball to powder ratio of 10:1, and with 9 cycles lasting 20 min spaced out with pauses of 10 min. 10 mL of hexane was used as milling medium (Sigma Aldrich purity of 98.5%). Open die pressing process [17] was employed for simultaneous synthesis and consolidation of tetrahedrite powders, permitting the obtaining of samples with size of about 4 cm^2 and thickness up to 5 mm. The process was performed using iron annealed tubes as sheath material: to prevent reactions or contamination of the thermoelectric phase a layer of boron nitride (BN) was deposited on the internal surface of the tube. The composite billet was assembled and closed with aluminium caps under argon atmosphere to prevent possible oxidation of the thermoelectric powders. Since the highest operating temperature of ODP facility is 500 °C, the composite billets were processed with 12 tons at 470 °C for 5 min to prevent the formation of secondary phases into the material, as observed by other authors [11], and to guarantee the absence of diffusion phenomena through the BN protective layer. In order to promote the phase evolution and sintering during ODP process a pre-heating cycle at higher temperature (520 °C, 10 min in a chamber furnace) was performed. The process parameters were set in order to have an overall time below 1.5 h, including the cooling step and the sheath removal.

The crystalline phases of ground samples were revealed by X-ray diffraction (XRD) using a PANalytical X'Pert Pro diffractometer with Bragg-Brentano geometry and Cu Kα radiation. The system is equipped with a thermal chamber (HTK1200N) able to reach 1200 °C in a controlled atmosphere (inert gas or vacuum), here used for the analyses up to 400 °C. XRD analyses were performed at room temperature (in air) and as a function of temperature, collecting the pattern at 50, 100, 200, 250, 300, and 400 °C employing a temperature ramp of 50 °C min^{-1} and maintaining the samples under He pressure of 0.05 MPa. The phase

identification of the XRD patterns was carried out employing Match! software (version 3.2.1 70) exploiting inorganic crystal structure database (ICSD, version 2016/1). The Rietveld refinement, performed by MAUD software [21], on the XRD profiles were exploited to obtain information of phase amounts, crystallite sizes and theoretical densities of samples [22]. The pellet densities were estimated through the geometrical method with a resulting error of 2% of the relative density values.

The morphological and quantitative compositional characterizations were performed by Sigma Zeiss field emission scanning electron microscope (FE-SEM) equipped with Oxford X-Max energy dispersive X-Ray spectroscopy (EDS) system. The EDS point analyses were carried out onto polished and carbon coated samples at 20 kV accelerating voltage, with acquisition time of 50 s, employing software INCA 4.14 (Oxford Instruments). The software was calibrated for quantification using the following standards referenced to a Co optimization standard (99.995%, Alpha Aesar USA, purchased by Astimex Standards): sphalerite ZnS (synthetic, S 32.91 wt%, Fe 0.01 wt%, Zn 67.07 wt%, Sn 0.01 wt%, Cerac Inc. USA), Copper Cu (99.999 wt% Johnson Matthey Chemicals, UK), and Nickel (99.97 wt%, Alpha Aesar, USA) purchased by SPI Supplies, and stibnite Sb_2S_3 (S 28.300 wt%, Sb 71.700 wt%, Cameca standards). The number of the cations was based on a unit formula of 29 and calculated maintaining the number of S atoms fixed to 13 [4,23,24]. The respective errors were calculated as the standard deviations of the measures.

Simultaneous thermogravimetric and differential scanning calorimetry analysis (TG-DSC) were carried out on crushed pellet powders (≈10 mg on alumina crucibles) by means of SDT Q 600 Apparatus (TA Instrument) from room temperature to 600 °C under synthetic nitrogen flow (rate 100 mL/min), with a heating rate of 10 °C/min.

The thermal diffusivity of the samples was measured by a laser flash thermal diffusivity apparatus (Netzsch LFA 457 MicroFlash®). The thermal conductivity κ was calculated according to the formula $\kappa = adC_p$ where a is the thermal diffusivity, d the density and C_p the specific heat of the material. The specific heat was calculated by means of the Netzsch Proteus Analysis software, comparing the samples with the standard material Netzsch Pyroceram 9606. The declared relative uncertainty was 3% for thermal diffusivity, and 5% for specific heat. The Seebeck coefficient, α, and the electrical resistivity, ρ, were measured in the temperature range from RT to 400 °C with a relative uncertainty of 5% and 10% respectively, using a customized test apparatus described elsewhere [25]. All measurements were carried out under Ar atmosphere with a heating ramp of 2.5 °C min^{-1}. The combined uncertainty for ZT resulted to be 20%.

3 Results and discussion

The influence of the stoichiometry, the synthesis conditions and the open die pressing process parameters on the tetrahedrite phase content, density, and thermoelectric properties of samples were investigated. In Fig. 1, the XRD pattern of sulfide precursors, prior and after ball milling treatment lasting 3, 12, and 24 h, are listed. As a first step, the employed precursor quantities were calculated in order to obtain a nominal stoichiometry of the final product of $Cu_{10}Zn_2Sb_4S_{13}$. The mechanical alloyed fraction increased with the increasing time, giving rise to the formation of the tetrahedrite phase up to a content close to 70 wt % after 24 h process.

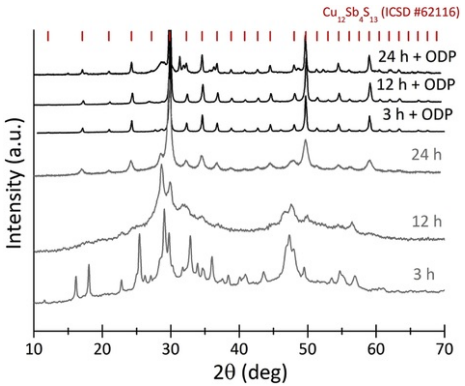

Fig. 1 XRD patterns of the $Cu_{10}Zn_2Sb_4S_{13}$ precursor powders after ball milling treatment for 3, 12, and 24 h and after ODP process.

alt-text: Fig. 1

After preliminary open die pressing consolidation process (pre-heating at 355 °C, processing with 35 tons at the same temperature and sintering at 355 °C for 20 min), different results depending on the starting powders were obtained. The powders milled for a shorter time (3 h and 12 h), showed a limited mechanical alloying and reacted during the sintering process giving rise to more than the 90 wt% of

tetrahedrite phase (ICSD 62116), with residual secondary phases identified as the orthorhombic Cu_3SbS_3 (ICSD #403111), $Cu_{7.2}S_4$ (ICSD #53330), and $CuSbS_2$ (ICSD #85133). Conversely the 24 h milled powders evolved during the sintering process to of a series of complex secondary phases arduous to be correctly resolved leading to a large uncertainty of the tetrahedrite phase quantification in the sintered sample. These preliminary results suggested limiting as much as possible the mechanical alloying, detrimental for the ODP simultaneous synthesis and sintering process. Being the 3 and 12 h treated powder results substantially comparable after ODP process, the shortest milling time (3 h) was chosen in order to reduce the whole process time.

To evaluate the effect of Zn content on material properties, four $Cu_{10}Cu_{1-x}Ni_1Zn_xSb_4S_{13}$ compositions with x = to 0.0, 0.3, 0.5, 0.7 were prepared starting from the best performing one, $Cu_{10}Cu_{0.5}Ni_1Zn_{0.5}Sb_4S_{13}$ [11]. Different pre-heating and pressing ODP temperature were explored and the preparation conditions were chosen maintaining the shortest milling time. The powders were ball milled for 3 h at 350 rpm in order to limit the mechanical alloying and the ODP conditions were chosen with a preheating at 520 °C for 10 min and then a pressing with 12 tons at 470 °C for 5 min. Fig. 2 depicted, as an example, an obtained pellet after the ODP process.

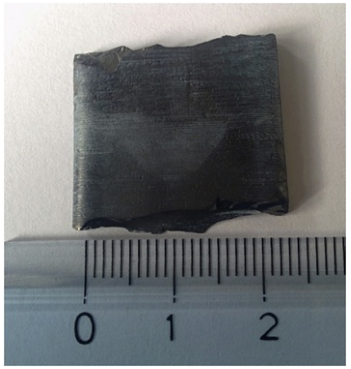

Fig. 2 Tetrahedrite pellet obtained by ODP process as it is after iron sheath removal.

alt-text: Fig. 2

As it is possible to observe by the XRD patterns listed in Fig. 3, after ODP treatment, all samples possessed the single tetrahedrite phase, with the exception of the sample with x = 0.7, which showed low intensity unknown peaks at 29.3°, 33.7°, 34.2°. Otherwise, the blank sample XRD pattern appeared more complicated if compared to the other samples. Indeed, in addition to the presence of orthorhombic Cu_3SbS_3 (ICSD #403111) and CuS (ICSD #32106), it resulted an overlapping of several very similar phases, likely $Cu_{12}Sb_4S_{13}$ (ICSD #62112, Cu-poor tetrahedrite(ICSD # 41753), and cubic Cu_3SbS_3 (ICSD #53332), which can be considered as a sub-stoichiometric tetrahedrite [26].

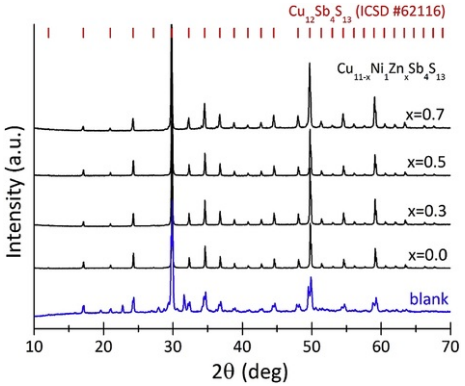

Fig. 3 XRD patterns of the sample obtained after ODP process at 470 °C for 5 min.

alt-text: Fig. 3

Unfortunately, sample x = 0.0, 0.3 and 0.5 broke up immediately after iron sheath removal, probably due to high internal stresses. This effect could be due to the difference in thermal expansion coefficients between the metallic sheath and the thermoelectric material: during the cooling after the sintering process, the larger contraction of the Fe external layer introduces a mechanical stress into the inner material, leading to the final fragile behavior of the pellets. Blank sample and the one with x = 0.7 showed good mechanical properties enough to allow the functional characterization. It was possible to characterize sample with x = 0.0 as well, even though broken. The calculated relative densities resulted to be 93%, 97%, 92% and 90% for x = 0.0, 0.3, 0.5, and 0.7 samples respectively. Observing secondary electron SEM micrographs listed in Fig. 4 (a, b, c, d, e), it is possible to assert that the blank sample possessed a relative density above the other sample ones. Moreover, it is worth noting that the Zn adding seemed to affect the grain size, which appeared less homogenous and smaller with Zn content increasing.

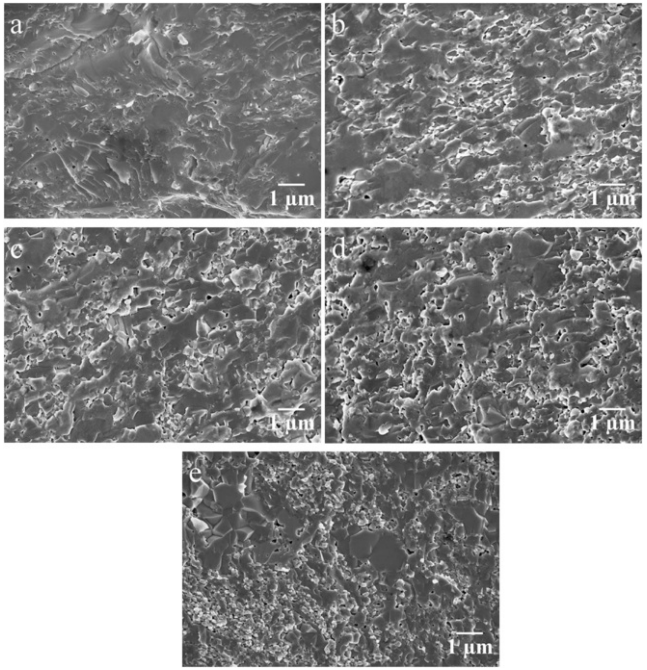

Fig. 4 Secondary electron micrographs of the fractured ODP samples: a) blank; b) x = 0.0; c) 0.3; d) 0.5 e) 0.7.

alt-text: Fig. 4

EDS stoichiometric quantifications, listed in Table 1, highlighted lower Cu contents than expected, probably due to the tetrahedrite tendency to deviate from the stoichiometry, in particular when substituted [23,27]. In the case of sample x = 0.7, the stoichiometry discrepancy is consistent with the presence of the different secondary phases detected by XRD. Otherwise, it is not possible to quantitatively evaluate the blank sample stoichiometry due to the presence of cubic Cu_3SbS_3 phase, which corresponds to a tetrahedrite sub-stoichiometric phase.

Table 1 Tetrahedrite phase stoichiometry results of the ODP samples obtained by EDS analyses.

alt-text: Table 1

Sample nominal stoichiometry $Cu_{11-x}Ni_1Zn_xSb_4S_{13}$	EDS tetrahedrite stoichiometry				
	Cu	Ni	Zn	Sb	S
Blank	–			–	<13.0
x = 0.0	10.3 ± 0.2	0.9 ± 0.1	–	4.0 ± 0.1	13.0

x = 0.3	10.6 ± 0.1	0.9 ± 0.1	0.3 ± 0.1	4.1 ± 0.1	13.0
x = 0.5	10.1 ± 0.1	0.9 ± 0.1	0.5 ± 0.1	4.0 ± 0.1	13.0
x = 0.7	9.9 ± 0.1	0.8 ± 0.1	0.6 ± 0.1	4.0 ± 0.1	13.0

In order to enhance the mechanical properties of the material, thus permitting an extensive functional characterization, a new sample series was prepared with the nominal stoichiometry of x equal to 0.3, 0.5, 0.7, 1.0. The same route conditions of the previous series were employed, but introducing a Ni excess as a binder additive by means of a 15 wt% of Ni_3S_2 precursor excess: the resulting S sub-stoichiometry was not completely compensated in order to obtain an excess of Ni. Indeed, the presence of small quantities of metals can enhance the sintering process of materials [28]. The choice of such element, instead of Cu and Zn, was mainly justified by its slighter influence on the tetrahedrite resistivity compared to the other metals present in the tetrahedrite [11]. Moreover, its role as a binder resulted clear being the stoichiometry unchanged among the two sets of samples.

Table 2 lists a summary of the prepared samples characteristics: the respective tetrahedrite phase contents were obtained by the Rietveld refinement of the XRD patterns (Fig. 5), collected at 50 °C. As previously observed, the tetrahedrite content augmented with the Cu substitution by Zn up to x = 0.5. For higher contents, the tetrahedrite phase decreased. The main secondary phases were NiSbS which was 4 wt% for all samples, and tetragonal Cu_2S (ICSD #16550) about 2–4 wt%, as already observed by other authors [29]. As an example, Fig. 6 depicted FE-SEM backscattered electron micrograph of a polished sample with x = 0.5 where the two phases, NiSbS (brighter phase) and Cu_2S (darker phase) can be easily distinguished.

Table 2 Blank and Ni-rich samples and their tetrahedrite phase features obtained by refinements of XRD patterns (collected at 50 °C).

alt-text: Table 2

Sample nominal stoichiometry $Cu_{11-x}Ni_1Zn_xSb_4S_{13}$	Tetrahedrite content (wt%)	Goodness of Rietveld refinement	Sample relative density (%)
Blank	78	1.8	94 ± 2
Ni-rich x = 0.3	94	2.2	88 ± 2
Ni-rich x = 0.5	95	2.6	91 ± 2
Ni-rich x = 0.7	93	1.6	90 ± 2
Ni-rich x = 1.0	91	2.2	95 ± 2

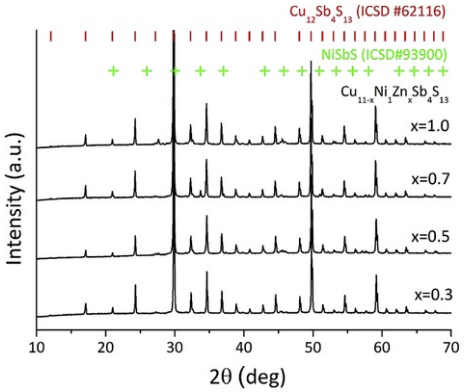

Fig. 5 XRD patterns (collected at 50 °C) of the Ni-rich samples obtained after ODP process.

alt-text: Fig. 5

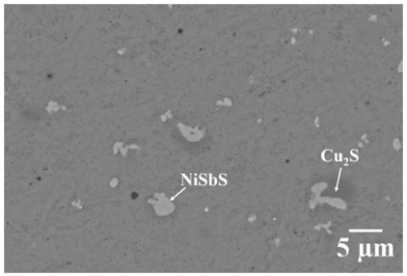

Fig. 6 Backscattered electron micrograph of the polished Ni-rich sample with x = 0.5 as an example: EDS analysis identified the brighter phase as NiSbS, while the darker one as Cu_2S (black spots were confirmed to be polishing residues containing Al, Si and O).

alt-text: Fig. 6

The density of the samples seemed to increase with Zn content and not to be affected by the Ni_3S_2 excess (comparing the results with those of previous sample series). Fig. 7 (a, b, c, and d) depicts secondary electron SEM micrographs of the Ni-rich samples, confirming the relative densities obtained by XRD Rietveld refinements.

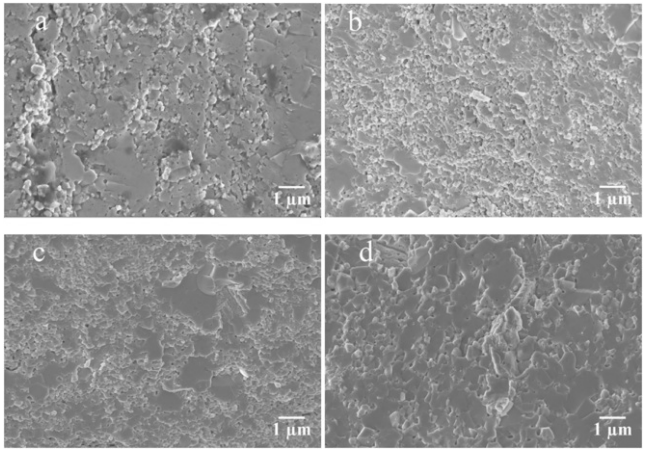

Fig. 7 Secondary electron micrographs of the fractured Ni-rich ODP samples: a) x = 0.3; b) x = 0.5; c) x = 0.7; d) x = 1.1.

alt-text: Fig. 7

Nevertheless, the Ni excess seemed to stabilize mechanically samples with x ≥ 0.5. Conversely, sample x = 0.3 would likely need higher Ni excess content to improve its mechanical properties properly.

EDS stoichiometric quantifications, listed in Table 3, highlighted a good accordance between measured and nominal compositions. Ni excess seemed to be concentrated into the secondary phases. Furthermore, its content in tetrahedrite phase appears to be lower than expected, decreasing with the increasing of Zn content.

Table 3 Tetrahedrite phase stoichiometry results of the Ni-rich ODP samples obtained by EDS analyses.

alt-text: Table 3

Sample nominal stoichiometry $Cu_{11-x}Ni_1Zn_xSb_4S_{13}$	EDS tetrahedrite stoichiometry				
	Cu	Ni	Zn	Sb	S
Ni-rich x = 0.3	11.0 ± 0.2	0.9 ± 0.1	0.3 ± 0.1	4.1 ± 0.1	13.0

Ni-rich x = 0.5	10.8 ± 0.2	0.9 ± 0.1	0.5 ± 0.1	4.1 ± 0.1	13.0
Ni-rich x = 0.7	10.7 ± 0.1	0.8 ± 0.1	0.7 ± 0.1	4.1 ± 0.1	13.0
Ni-rich x = 1.0	10.1 ± 0.3	0.7 ± 0.1	0.9 ± 0.1	4.1 ± 0.1	13.0

XRD analyses of blank (Fig. 8) and Ni-rich ODP samples were performed as a function of temperature (under inert atmosphere) up to 400 °C (Fig. 9, which reports Ni-rich ODP sample with x = 0.5 as an example). Blank sample possessed several phases, such as $Cu_{12}SbS_{13}$ (ICSD #62112), cubic Cu_3SbS_3 (ICSD #32106), orthorhombic Cu_3SbS_3 (ICSD #403111), and CuS (ICSD #32106). At 400 °C it became a tetrahedrite single phase. After the whole thermal cycle at 50 °C, it showed 50 wt% of cubic Cu_3SbS_3 (ICSD # 53332) in addition to 37 wt% of tetrahedrite one (ICSD #62112), at 50 °C. In Fig. 10, the XRD patterns of the samples at 50 °C after the thermal cycle are shown. In particular, it is worth noting that NiSbS disappeared by all sample (but the sample with 0.7, which maintained roughly few weight percent), partially giving rise to the formation of hexagonal NiS (ICSD # 42494). The phases were also detected by other authors [12], even if they observed the formation of NiSbS phase only after 520 °C.In particular, such transformation occurred after 300 °C, as it is possible to observe by Fig. 8. In general, other phases with few weight percent appeared Sb_2O_3 (ICSD #16851) with a visible peak at 27.6°, Cu_2S with cubic (ICSD #202785) and hexagonal (ICSD #200987) symmetries.

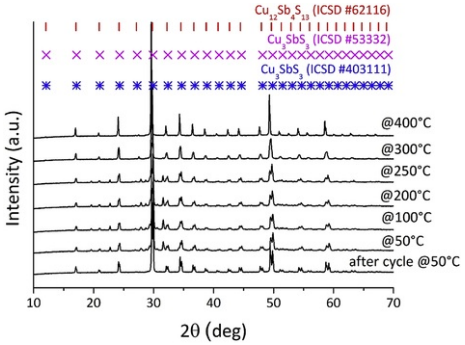

Fig. 8 XRD patterns obtained at different temperatures of the blank sample.

alt-text: Fig. 8

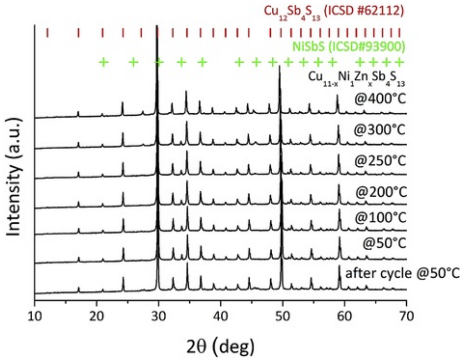

Fig. 9 XRD patterns obtained at different temperatures of the Ni-rich ODP sample with x = 0.5.

alt-text: Fig. 9

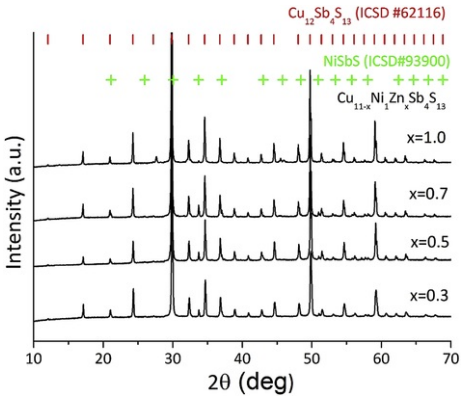

Fig. 10 XRD patterns (collected at 50 °C) of the Ni-rich ODP samples obtained after thermal cycle.

alt-text: Fig. 10

It was possible to perform a complete thermoelectric characterization for blank, x = 0 and x = 0.7 sample pellets of the first series, and for all pellets of the second series (the Ni-rich one) but the one with x = 0.3. Anyway, electrical resistivity and Seebeck coefficients were measured also for samples with x = 0.5 and Ni-rich x = 0.3.

The observed trend of Seebeck coefficients (Fig. 11) and electrical resistivities (Fig. 12) (measured between RT and 400 °C) were fully in agreement with those previously reported [3,11]. The absolute values of the Seebeck coefficient depended on the chemical composition. Due to the substitution of Cu with Zn, additional electron filled the valence hole states pushing the Fermi level to the top of the valence band, reducing the charge carrier density [11], and giving rise to the increasing of the values of Seebeck coefficient and electrical resistivity. In particular, $|\alpha|$tended to increase in the whole temperature range for x = 0.5, x = 0.7, Ni-rich x = 0.5, Ni-rich x = 0.7, consistently with the fact that the difference between the Fermi level and the energy of the valence band decreased with T and could even move slightly into the gap. Blank and Ni-rich x = 1.0 samples, showed a different trend below 150 °C: indeed, the Seebeck coefficient values slightly decreased with temperature in that range. It is worth noting that the x = 0 sample possessed higher Seebeck coefficient values but lower resistivity with respect to the blank sample. As reported by Suekuni et al. [10], α increased within Ni content, while Lu et al. [11] suggested that each substitutional Ni introduced one hole level to the valence band of the host, maintaining the band structure almost metallic. It was assumed that the increased number of heavy mass holes enhanced the absolute value of the Seebeck coefficient [10] while both holes and electrons affected the electrical conduction increasing resistivity values. In this case, the presence of secondary phases in the blank sample could result in an increase of the electrical resistivity, explaining why these values are greater than those measured for sample x = 0. An estimation of the charge carrier density and mobility could be very useful to understand these complex behaviors but, as already reported by other authors, Hall effect measurement on these kind of materials are really difficult to perform, due to the very small Hall response [23,30].

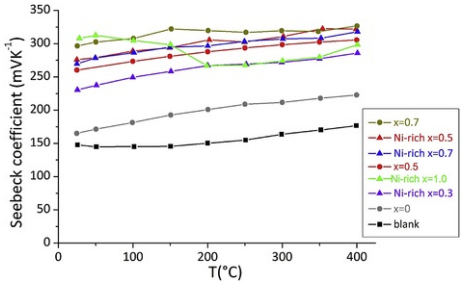

Fig. 11 Seebeck coefficient values of samples as a function of temperature.

alt-text: Fig. 11

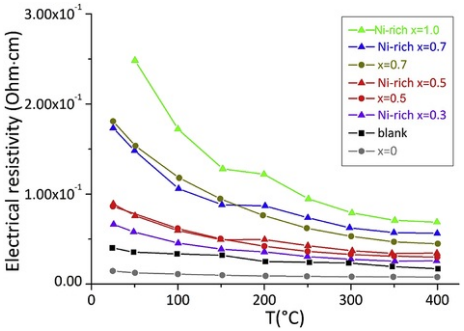

Fig. 12 Electrical resistivity of the samples as a function of temperature.

alt-text: Fig. 12

The change of the electrical conductivity slope observed around 200 °C for all Ni-rich samples was investigated using TG-DSC analyses on pellet samples previously ground (Fig. 13). The analyses displayed a change in the slope of the DSC curves close to 200 °C on the Ni-rich samples while no changes were observed for blank sample. This downward weak deflection in the DSC signal could be attributable to second order transitions related to the magnetism of Ni-based compounds, such as the ferromagnetic or antiferromagnetic/paramagnetic transitions. Usually the DSC signals for these processes are weak and sometimes not easy to detect [31]. This could be the reason why for samples x = 0.0 and = 0.5 that deflection is not visible at the measurement conditions employed. The magnetic transitions could be responsible for the anomalous trend on the Seebeck coefficient of Ni rich x = 1 sample, where it abruptly decreased in the 150–200 °C range.

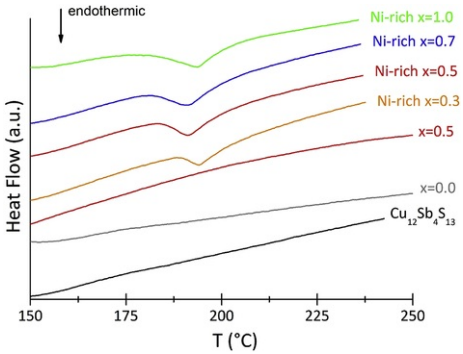

Fig. 13 Differential scanning calorimetry analysis of the samples crashed pellet powder under N_2 flux.

alt-text: Fig. 13

The thermal conductivity (Fig. 14) of the blank and x = 0 samples increased with the temperature showing higher values as expected by the lower electrical resistivity. Conversely, the thermal conductivity for co-doped samples did not significantly increased with the temperature. This is consistent with the trend of the electrical resistivity, reflecting the reduction of the electronic contribution to the thermal transport which is more temperature-dependent [11]. The substitution of Cu with Zn and Ni was expected to further contribute in decreasing the lattice thermal conductivity due to the improved phonon scattering process. In particular, the efficiency in reducing thermal conductivity seemed to increase with the disorder of the system. In fact, the substitution of Cu with Zn acted both removing carriers from the system and introducing disorder on the Cu(1) site. This effect reached its maximum when the Zn content was in such a way to move the system out of a lattice symmetric configuration. This could explain the discrepancy observed between electrical and thermal conductivities results for the x = 1 sample. Indeed, in the x = 1 sample, the Cu substituted sites are exactly half occupied by Ni and Zn cations increasing the order of the system and giving rise to a slightly higher lattice thermal conductivity as respect to x = 0.5 and x = 0.7.

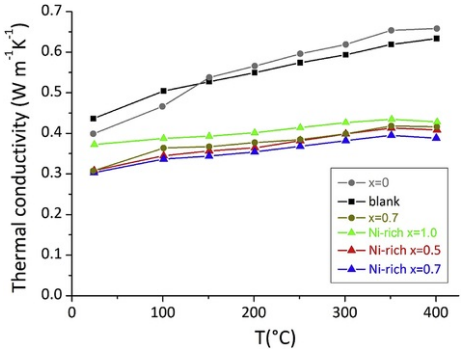

Fig. 14 Thermal conductivity of samples as a function of temperature.

alt-text: Fig. 14

Combining the measured physical characteristics, it is possible to observe the adimensional figure of merit of the samples (Fig. 15). In particular, it is worth noting that blank sample ZT values resulted slightly lower than those published before [3,10,12], even if they are comparable taking into account the large intrinsic error of ZT estimation. Sample x = 0.7 and the Ni-rich x = 0.7 did not show large differences in the thermoelectric properties (Seebeck coefficients, electrical and thermal conductivities) giving rise to very similar thermoelectric figure of merit. Among the co-doped samples, the Ni-rich x = 0.5 possessed a maximum value of 0.48 at 400 °C. Like in the blank sample case, this latter result was lower than those (close to 0.9 at the same temperature) reported in literature for the same tetrahedrite phase stoichiometry [11]. The highest improvement of ZT was obtained for x = 0, with a ZT of 0.65 at 400 °C, even though it was mechanically unstable. That value can be considered compatible, within the experimental error, with the result obtained on a slightly different composition prepared with a similar synthesis route [14]. Moreover, those ZT results were certainly affected by the lack of density of pellets (around 90%), the lower content of Ni in the tetrahedrite phase, and the presence of several secondary phases, even though limited to few weigh percent.

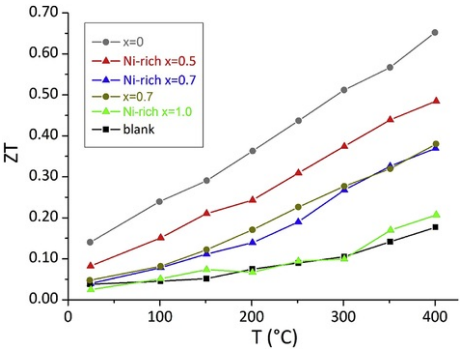

Fig. 15 Figure of merit of samples as a function of temperature.

alt-text: Fig. 15

4 Conclusions

In this work, thermoelectric tetrahedrite pellets were obtained with both Zn and Ni cations as partial substituents of Cu by a ball milling pre-treatment of sulphur powder precursors and a successive fast one-step simultaneous synthesis and sintering by ODP. The mechanical stability of the pellets was reached for the stoichiometry $Cu_{11-x}Ni_1Zn_xSb_4S_{13}$ with x ≥ 0.5 introducing 15 wt% of the precursor Ni_3S_2, and avoiding to completely compensate the S sub-stoichiometry in order to have an excess of Ni. The latter seemed to not substantially increase its content inside the tetrahedrite phase, which was characterized by quantitative EDS analyse, but to decrease it by giving rise to the presence of several secondary phases. The presence of the dopants decreased lattice thermal conductivity due to the phonon scattering process, and increased Seebeck coefficient and electrical resistivity. This gave rise to an improvement of ZT from 0.20 of the undoped blank sample to 0.48 at 400 °C for the sample x = 0.5, which possessed good mechanical stability, even if it resulted lower than the one reported in literature for the same phase stoichiometry [11]. The highest improvement of ZT was obtained for x = 0 sample with a ZT of 0.65 at 400 °C, even though it lacked of mechanical

stability, being however compatible within the experimental error with the result obtained on a slightly different composition prepared with a similar synthesis route [14].

This work demonstrated that it is possible to obtain tetrahedrite pellets with size of some centimetres with a good mechanical stability using simple and cheap processes, following fast routes (lasting less than 6 h), potentially easily scalable up to the production of pellets with the size of tens of centimetres. Moreover, the thermoelectric performance of the material produced, slightly lower than the best ones reported in literature, does not prevent the ODP based production route by an industrial application since, nowadays, a n-type thermoelectric leg compatible with tetrahedrite based p-type leg, such as Mg_2Si [28] or TiS_2 [16], still lack of a figure of merit higher than the one presented in this work.

Acknowledgments

The authors are grateful to Stefano Boldrini (CNR-ICMATE) and Filippo Agresti (CNR-ICMATE) for the valuable discussion about the results, to Enrico Bassani (CNR-ICMATE) for his essential technical supports, Dr Corrado Tommasi (CNR-ICMATE) for valuable discussion about the DSC, and Raul Carampin (CNR-IGG) for the inestimable help, advices and data discussion about the quantitative EDS analyses.

This work has been funded by the Italian National Research Council - Italian Ministry of Economic Development Agreement “Ricerca di sistema elettrico nazionale”.

Appendix A. Supplementary data

Supplementary data related to this article can be found at http://dx.doi.org/10.1016/j.jallcom.2017.01.187.

References

[1] S. LeBlanc, Thermoelectric generators: linking material properties and systems engineering for waste heat recovery applications, *Sustain. Mater. Technol.* **1–2**, 2014, 26–35, http://dx.doi.org/10.1016/j.susmat.2014.11.002.

[2] X. Lu and D.T. Morelli, Natural mineral tetrahedrite as a direct source of thermoelectric materials, *Phys. Chem. Chem. Phys.* **15**, 2013, 5762–5766, http://dx.doi.org/10.1039/c3cp50920f.

[3] X. Lu, D.T. Morelli, Y. Xia, F. Zhou, V. Ozolins, H. Chi, X. Zhou and C. Uher, High performance thermoelectricity in earth-abundant compounds based on natural mineral tetrahedrites, *Adv. Energy Mater* **3**, 2013, 342–348, http://dx.doi.org/10.1002/aenm.201200650.

[4] S. Fadda, M. Fiori and S.M. Grillo, Chemical variations in tetrahedrite - tennantite Chemical variations in tetrahedrite-tennantite minerals from the Furtei epithermal Au deposit, Sardinia, Italy: mineral zoning and ore fluids evolution, In: *Au-Ag-Te-Se Depos. IGCP Proj,* 2005, 79–84.

[5] J. Wang, M. Gu, Y. Bao, X. Li and L. Chen, Quick fabrication and thermoelectric properties of Cu12Sb4S13 tetrahedrite, *J. Electron. Mater* **45**, 2016, 2274–2277, http://dx.doi.org/10.1007/s11664-015-4301-8.

[6] S. Fasolin, S. Fiameni, C. Fanciulli, S. Battiston, A. Famengo and M. Fabrizio, Nanostructured tetrahedrite synthesis for thermoelectric applications, *J. Nanosci. Nanotechnol.* **7**, 2017, 1645–1649, http://dx.doi.org/10.1166/jnn.2017.13733.

[7] F. Di Benedetto, G.P. Bernardini, C. Cipriani, C. Emiliani, D. Gatteschi and M. Romanelli, The distribution of Cu(II) and the magnetic properties of the synthetic analogue of tetrahedrite: Cu12Sb4S13, *Phys. Chem. Min.* **32**, 2005, 155–164, http://dx.doi.org/10.1007/s00269-005-0449-8.

[8] N.E. Jonnson, J.R. Craig and J.D. Rimstidt, Crystal chemistry of tetrahedrite, *Am. Mineral.* **73**, 1988, 389–397.

[9] K. Friese, A. Grzechnik, E. Makovicky, T. Balic-Zunic and S. Karup-Møller, Crystal structures of iron bearing tetrahedrite and tennantite at 25 and 250 degrees C by means of Rietveld refinement of synchrotron data, *Phys. Chem. Min.* **35**, 2008, 455–465, http://dx.doi.org/10.1007/s00269-008-0240-8.

[10] K. Suekuni, K. Tsuruta, M. Kunii, H. Nishiate, E. Nishibori, S. Maki, M. Ohta, A. Yamamoto and M. Koyano, High-performance thermoelectric mineral Cu12-xNi xSb4S13 tetrahedrite, *J. Appl. Phys.* **113**, 2013, http://dx.doi.org/10.1063/1.4789389.

[11] X. Lu, D.T. Morelli, Y. Xia and V. Ozolins, Increasing the thermoelectric figure of merit of tetrahedrites by Co-doping with nickel and zinc, *Chem. Mater* **27**, 2015, 408–413, http://dx.doi.org/10.1021/cm502570b.

[12] T. Barbier, P. Lemoine, S. Gascoin, O.I. Lebedev, A. Kaltzoglou, P. Vaqueiro, A.V. Powell, R.I. Smith and E. Guilmeau, Structural stability of the synthetic thermoelectric ternary and nickel-substituted tetrahedrite

phases, *J. Alloys Compd.* **634**, 2015, 253–262, http://dx.doi.org/10.1016/j.jallcom.2015.02.045.

[13] R. Chetty, P.K.D.S.G. Rogl, P. Rogl, E. Bauer, H. Michor, S. Suwas, S. Puchegger, G. Giester and R.C. Mallik, Thermoelectric properties of a Mn substituted synthetic tetrahedrite, *Phys. Chem. Chem. Phys.* **17**, 2015, 1716–1727, http://dx.doi.org/10.1039/C4CP04039B.

[14] R. Chetty, A. Bali, M.H. Naik, G. Rogl, P. Rogl, M. Jain, S. Suwas and R.C. Mallik, Thermoelectric properties of Co substituted synthetic tetrahedrite, *Acta Mater* **100**, 2015, 266–274, http://dx.doi.org/10.1016/j.actamat.2015.08.040.

[15] T. Barbier, S. Rollin-Martinet, P. Lemoine, F. Gascoin, A. Kaltzoglou, P. Vaqueiro, A.V. Powell and E. Guilmeau, Thermoelectric materials: a new rapid synthesis process for nontoxic and high-performance tetrahedrite compounds, *J. Am. Ceram. Soc.* **99**, 2016, 51–56, http://dx.doi.org/10.1111/jace.13838.

[16] T. Barbier, P. Lemoine, S. Martinet, M. Eriksson, M. Gilmas, E. Hug, G. Guélou, P. Vaqueiro, A.V. Powell and E. Guilmeau, Up-scaled synthesis process of sulphur-based thermoelectric materials, *RSC Adv.* **6**, 2016, 10044–10053, http://dx.doi.org/10.1039/C5RA23218J.

[17] S. Ceresara, C. Fanciulli, F. Passaretti and D. Vasilevskiy, Texturing of (Bi0.2Sb0.8)2Te3 nanopowders by open die pressing, *J. Electron. Mater* **42**, 2013, 1529–1534, http://dx.doi.org/10.1007/s11664-012-2313-1.

[18] S. Battiston, S. Boldrini, M. Saleemi, A. Famengo, S. Fiameni, M.S. Toprak and M. Fabrizio, Influence of Al and Mg addition on thermoelectric properties of higher manganese silicides obtained by reactive sintering, *J. Nanosci. Nanotechnol.* **17**, 2017, 1668–1673, http://dx.doi.org/10.1166/jnn.2017.13730.

[19] A. Famengo, S. Battiston, M. Saleemi, S. Boldrini, S. Fiameni, F. Agresti, M.S. Toprak, S. Barison and M. Fabrizio, Phase content influence on thermoelectric properties of manganese silicide-based materials for middle-high temperatures, *J. Electron. Mater.* **42**, 2013, 2020–2024, http://dx.doi.org/10.1007/s11664-013-2507-1.

[20] C. Fanciulli, S. Battiston, S. Boldrini, E. Villa, A. Famengo, S. Fiameni, M. Fabrizio and F. Passaretti, Fast sintering of thermoelectric silicide powders using open die pressing technique, *Mater. Today Proc.* **2**, 2015, 566–572, http://dx.doi.org/10.1016/j.matpr.2015.05.077.

[21] L. Lutterotti, S. Matthies, H.R. Wenk, A.S. Schultz and J.W. Richardson, Jr., Combined texture and structure analysis of deformed limestone from time-of-flight neutron diffraction spectra, *J. Appl. Phys.* **81**, 1997, 594, http://dx.doi.org/10.1063/1.364220.

[22] L. Lutterotti, D. Chateigner, S. Ferrari and J. Ricote, Texture, residual stress and structural analysis of thin films using a combined X-ray analysis, *Thin Solid Films* **450**, 2004, 34–41, http://dx.doi.org/10.1016/j.tsf.2003.10.150.

[23] Y. Bouyrie, S. Sassi, C. Candolfi, J.-B. Vaney, A. Dauscher and B. Lenoir, Thermoelectric properties of double-substituted tetrahedrites Cu12-xCoxSb4-yTeyS13, *Dalt. Trans.* **45**, 2016, 7294–7302, http://dx.doi.org/10.1039/C6DT00564K.

[24] A.R. McKinnon, A Geochemical Exploration Model for Ore Deposits in the Cobar Basin, 2007, PhD Thesis Univ. West; Sydney.

[25] S. Boldrini, A. Famengo, F. Montagner, S. Battiston, S. Fiameni, M. Fabrizio and S. Barison, Test rig for high-temperature thermopower and electrical conductivity measurements, *J. Electron. Mater* **42**, 2013, 1319–1323, http://dx.doi.org/10.1007/s11664-012-2437-3.

[26] B.J. Wuensch, Confirmation of the crystal structure of tetrahedrite, Cu12Sb4S13, *Sci. (80-.)* **141**, 1963, 804–805.

[27] M.L. Johnson and R. Jeanloz, A brillouin-zone model for compositional variation in tetrahedrite, *Am. Mineral.* **68**, 1983, 220–226.

[28] T. Sakamoto, A. Famengo, S. Barison, S. Battiston, S. Boldrini, A. Ferrario, S. Fiameni, T. Iida, Y. Takanashi and M. Fabrizio, Structural, compositional and functional properties of Sb-doped Mg2Si synthesized in Al2O3-crucibles, *RSC Adv.* **6**, 2016, 105–114, http://dx.doi.org/10.1039/C6RA11367B.

[29] R. Chetty, A. Bali and R.C. Mallik, Tetrahedrites as thermoelectric materials: an overview, *J. Mater. Chem. C* **3**, 2015, 12364–12378, http://dx.doi.org/10.1039/c5tc02537k.

[30] Y. Bouyrie, C. Candolfi, V. Ohorodniichuk, B. Malaman, A. Dauscher, J. Tobola and B. Lenoir, Crystal structure, electronic band structure and high-temperature thermoelectric properties of Te-substituted

tetrahedrites $Cu_{12}Sb_{4-x}Te_xS_{13}$ ($0.5 \le x \le 2.0$), *J. Mater. Chem. C* **3**, 2015, 10476–10487, http://dx.doi.org/10.1039/C5TC01636C.

[31] H.W. Williams and B.L. Chamberland, Determination of Curie, nhel, or crystallographic transition temperatures via differential scanning calorimetry, *Anal. Chem.* **41**, 1969, 2084–2086, http://dx.doi.org/10.1063/1.438208.

Appendix A. Supplementary data

The following is the supplementary data related to this article:

Multimedia Component 1

Graphical abstract

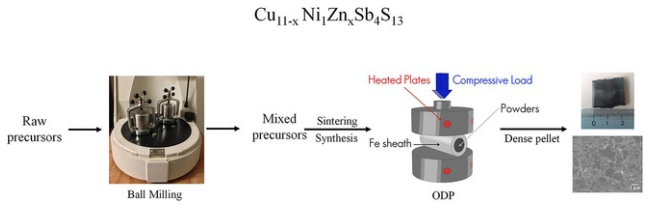

alt-text: Image 1

Highlights

- New and scalable synthesis and sintering route for tetrahedrite based thermoelectric materials.
- Whole process lasted less than 6 h.
- Zn and Ni addition influence on tetrahedrite stability and thermoelectric properties.

Queries and Answers

Query: Could you please provide the grant number for Ricerca di sistema elettrico nazionale, if any?
Answer: No, this project does not have a grant number

Query: Please confirm that given names and surnames have been identified correctly.
Answer: All correct

Query: Your article is registered as a regular item and is being processed for inclusion in a regular issue of the journal. If this is NOT correct and your article belongs to a Special Issue/Collection please contact san.natarajan@elsevier.com immediately prior to returning your corrections.
Answer: regular issue